ELSEVIER

Information Fusion 2 (2001) 177–186

INFORMATION FUSION

www.elsevier.com/locate/inffus

A new look at IHS-like image fusion methods

Te-Ming Tu, Shun-Chi Su, Hsuen-Chyun Shyu, Ping S. Huang *

Department of Electrical Engineering, Chung Cheng Institute of Technology, Taoyuan 33509, Taiwan, ROC

Received 12 January 2001; received in revised form 11 April 2001; accepted 23 April 2001

Abstract

The intensity-hue-saturation (IHS) method, principal component analysis (PCA), Brovey transform (BT) and wavelet transform (WT) are the contemporary image fusion methods in remote sensing community. However, they often face color distortion problems with fused images. In other words, they are sensitive to the characteristics of the analyzed area. To investigate this color distortion problem, this work presents a relatively detailed study indicating that the color distortion problem arises from the change of the saturation during the fusion process. Meanwhile, PCA, BT, and WT are evaluated and found to be IHS-like image merging techniques. Experimental results for distinct image fusion methods are also demonstrated in this paper. © 2001 Published by Elsevier Science B.V.

Keywords: Image fusion; Intensity-hue-saturation method; Principal component analysis; Brovey transform; Wavelet transform

1. Introduction

With the development of new imaging sensors a meaningful fusion method for all employed imaging sources becomes necessary. Image fusion is a novel means of combining the spectral information of a coarse-resolution image with the spatial resolution of a finer image. The resulting merged image is a product that synergistically combines the best features of each of its components. The benefit of merged image has been demonstrated in many practical applications, especially for vegetation, land-use, precision farming, and urban studies. For local environmental applications, the high-resolution CARTERRA images from the IKONOS satellite can now currently be acquired in two different modes: the panchromatic (Pan) mode with high spatial resolution of 1 m and the multispectral (MS) mode with a four times coarser ground resolution. To take the advantage of CARTERRA images, it is important to determine an optimum merging approach for the current task.

Various methods for image fusion [1–14] have been described earlier. According to their efficiency and implementation, intensity-hue-saturation (IHS) method [1–3], principal component analysis (PCA) [2,4] and Brovey transform (BT) [2,9] are most commonly used algorithms in remote sensing community. However, the problem of color distortion appears at the analyzed area after transformed by using these fusion methods. Compared to these methods, the wavelet transform (WT) with multiresolution decomposition [5–7,10–13] is a relatively new approach. The WT can characterize the local variance at different scales due to its changing resolutions in both the spatial and spectral domains.

Until now, these methods have only been independently evaluated by some statistical metrics and have seldom been compared quantitatively with each other, in both spectral and spatial features. For instance, all of the IHS, PCA, and BT can keep the same spatial resolution as the Pan image but distort the spectral (color) characteristics with different degree. In contrast to above methods, the WT is the easiest method to control the trade-off between the spatial and spectral information. However, WT method preserves more spectral information but looses more spatial information, this needs to be investigated. Under this background, the present work was initiated. A detailed study indicated that the color distortion problem arises from the change of the saturation during the fusion process. Experimental results for distinct fusion methods are also demonstrated in the present paper.

2. The RGB–IHS conversion model

Several different mathematical representations of the transformation can convert RGB tristimulus values into the parameters of human color perception and vice versa

* Corresponding author. Tel.: +886-3380-3552; fax: +886-3380-1407.

E-mail address: pshuang@ccit.edu.tw (P.S. Huang).

1566-2535/01/$ - see front matter © 2001 Published by Elsevier Science B.V.
PII: S1566-2535(01)00036-7

[14,15]. Beyond computational speed, these algorithms differ mainly in the choice of coordinate systems (cylindrical or spherical coordinates), the primary color used as the hue reference point, and the method used to calculate the intensity component of the transformations.

To understand the color distortion during the image fusion process, it is necessary to review two essential but important RGB–IHS conversion models. The first RGB–IHS conversion system is a linear transformation:

$$\begin{bmatrix} I \\ v1 \\ v2 \end{bmatrix} = \begin{bmatrix} 1/3 & 1/3 & 1/3 \\ -\sqrt{2}/6 & -\sqrt{2}/6 & 2\sqrt{2}/6 \\ 1/\sqrt{2} & -1/\sqrt{2} & 0 \end{bmatrix} \begin{bmatrix} R \\ G \\ B \end{bmatrix}$$

and

$$\begin{bmatrix} R \\ G \\ B \end{bmatrix} = \begin{bmatrix} 1 & -1/\sqrt{2} & 1/\sqrt{2} \\ 1 & -1/\sqrt{2} & -1/\sqrt{2} \\ 1 & \sqrt{2} & 0 \end{bmatrix} \begin{bmatrix} I \\ v1 \\ v2 \end{bmatrix}. \tag{1}$$

Variables $v1$ and $v2$ in (1) can be considered as x and y axes in the Cartesian coordinate system while intensity I indicates the z axis. In this way, the hue (H) and saturation (S) can be represented by:

$$H = \tan^{-1}\left(\frac{v2}{v1}\right) \quad \text{and} \quad S = \sqrt{v1^2 + v2^2}. \tag{2}$$

Alternately, we can rotate the RGB cube until the horizontal plane is parallel to the Maxwell triangle and the vertical axis lies on the gray line of the RGB cube. As such, a nonlinear RGB–IHS conversion system can be represented by [14]:

$$I = (R + G + B)/3 \tag{3a}$$

$$H = \begin{cases} \cos^{-1}(a) & \text{if } G \geqslant R, \\ 2\pi - \cos^{-1}(a) & \text{if } G \leqslant R, \end{cases} \qquad a = \frac{(2B - G - R)/2}{\sqrt{(B-G)^2 + (B-R)(G-R)}}, \tag{3b}$$

$$S = 1 - \frac{3\min(R, G, B)}{R + G + B}. \tag{3c}$$

These two RGB–IHS conversion systems differ mainly in their representations for the saturation. In (1) and (2), pixels with identical $\sqrt{v1^2 + v2^2}$ have the same saturation value which is independent of the intensity I. These pixel points form a saturation barrel in the IHS space. For the conversion system in (3a), (3b) and (3c), pixels with identical $\sqrt{v1^2 + v2^2}$ are located on the surface of a saturation cone with saturation values proportional to distinct intensities. Details of the relation between (1), (2), (3a), (3b) and (3c) have been reported by Ledley et al. [16].

3. A generalized IHS image fusion (GIHS)

To compare various image fusion methods in RGB–IHS space, we first introduce a unifying image fusion method called generalized IHS (GIHS). By using GIHS, the low-resolution intensity component (I_0) in IHS space is replaced by a gray-level image with higher spatial resolution (I_{new}) and transformed back into the original RGB space with the original H and S components in (2). That is,

Step 1:

$$\begin{bmatrix} I_0 \\ v1_0 \\ v2_0 \end{bmatrix} = \begin{bmatrix} 1/3 & 1/3 & 1/3 \\ -\sqrt{2}/6 & -\sqrt{2}/6 & 2\sqrt{2}/6 \\ 1/\sqrt{2} & -1/\sqrt{2} & 0 \end{bmatrix} \begin{bmatrix} R_0 \\ G_0 \\ B_0 \end{bmatrix}. \tag{4a}$$

Step 2: I_0 is replaced by I_{new}.

Step 3:

$$\begin{bmatrix} R_{\text{new}} \\ G_{\text{new}} \\ B_{\text{new}} \end{bmatrix} = \begin{bmatrix} 1 & -1/\sqrt{2} & 1/\sqrt{2} \\ 1 & -1/\sqrt{2} & -1/\sqrt{2} \\ 1 & \sqrt{2} & 0 \end{bmatrix} \begin{bmatrix} I_{\text{new}} \\ v1_0 \\ v2_0 \end{bmatrix}, \tag{4b}$$

where R_0, G_0, B_0, I_0, $v1_0$, and $v2_0$ represent the corresponding values for the resized original multispectral image. R_{new}, G_{new}, and B_{new} are corresponding values of the fused images.

Directly implementing of the GIHS method in (4a) and (4b) requires numerous multiplication and addition operations, making it computationally inefficient. To develop a computationally efficient method without the coordinate transformation, (4a) and (4b) can be rewritten as

$$\begin{aligned} \begin{bmatrix} R_{\text{new}} \\ G_{\text{new}} \\ B_{\text{new}} \end{bmatrix} &= \begin{bmatrix} 1 & -1/\sqrt{2} & 1/\sqrt{2} \\ 1 & -1/\sqrt{2} & -1/\sqrt{2} \\ 1 & \sqrt{2} & 0 \end{bmatrix} \begin{bmatrix} I_0 + (I_{\text{new}} - I_0) \\ v1_0 \\ v2_0 \end{bmatrix} \\ &= \begin{bmatrix} 1 & -1/\sqrt{2} & 1/\sqrt{2} \\ 1 & -1/\sqrt{2} & -1/\sqrt{2} \\ 1 & \sqrt{2} & 0 \end{bmatrix} \begin{bmatrix} I_0 + \delta \\ v1_0 \\ v2_0 \end{bmatrix} \\ &= \begin{bmatrix} R_0 + \delta \\ G_0 + \delta \\ B_0 + \delta \end{bmatrix}, \end{aligned} \tag{5}$$

where $\delta = I_{\text{new}} - I_0$. Eq. (5) states that the fused image $[R_{\text{new}}, G_{\text{new}}, B_{\text{new}}]^{\text{T}}$ can be easily obtained from the resized original image $[R_0, G_0, B_0]^{\text{T}}$, simply by addition. Hence, the GIHS method can be implemented efficiently.

A problem of the GIHS method (and also many other image fusion methods) is that the color of the image may be changed during fusion. This phenomenon is termed as color distortion problem here after. Numerous previous experiments also encountered this problem, indicating that the saturation of images fused by using Eq. (4b) is higher or lower than the original value in the multispectral image. Partitioning of Eq. (4b) gives, however,

$$\begin{bmatrix} R_{\text{new}} \\ G_{\text{new}} \\ B_{\text{new}} \end{bmatrix} = \begin{bmatrix} I_{\text{new}} \\ I_{\text{new}} \\ I_{\text{new}} \end{bmatrix} + \begin{bmatrix} -1/\sqrt{2} & 1/\sqrt{2} \\ -1/\sqrt{2} & -1/\sqrt{2} \\ \sqrt{2} & 0 \end{bmatrix} \begin{bmatrix} v1_0 \\ v2_0 \end{bmatrix} \tag{6}$$

reveals that both H and S defined by (2) are preserved during fusion. By substituting R_{new}, G_{new}, and B_{new} into (1), however, the new $v1$, and $v2$ rarely equal $v1_0$, and $v2_0$. Therefore, the saturation preserving property in (4b) produces a distorted hue and saturation values for the new (fused) image, a confused imperfection of the IHS-based method.

To discover how the hue and saturation change during the image fusion process, δ in Eq. (5) can be substituted into Eqs. (3b) and (3c) and the notations defined before can be adopted. Following image fusion, a in Eq. (3b) can be re-calculated as

$$\begin{aligned} a' &= \{(2(B_0+\delta)-(G_0+\delta)-(R_0+\delta))/2\} \\ &\quad \Big/ \Big\{((B_0+\delta)-(G_0+\delta))^2 + ((B_0+\delta)-(R_0+\delta)) \\ &\quad \times ((G_0+\delta)-(R_0+\delta))\Big\}^{1/2} \\ &= \frac{(2B_0-G_0-R_0)/2}{\sqrt{(B_0-G_0)^2+(B_0-R_0)(G_0-R_0)}} = a_0. \end{aligned} \tag{7}$$

Eq. (7) indicates that the hue H for the fused image using Eq. (3b) is unchanged, i.e., the same as that of the original multispectral color image, when I_0 is replaced by I_{new}. Therefore, the hue value in images fused by Eqs. (4a) and (4b) is always correct. In contrast, by using Eq. (3c), the saturation value for the resized original multispectral image can be given by

$$S_0 = 1 - \frac{3X_0}{R_0+G_0+B_0} = \frac{I_0 - X_0}{I_0}, \tag{8a}$$

where X_0 denotes the minimum value among R_0, G_0, B_0. By substituting δ and corresponding notations into Eq. (8a), the new saturation value for the fused image becomes

$$\begin{aligned} S' &= 1 - \frac{3\min(R_0+\delta, G_0+\delta, B_0+\delta)}{R_0+G_0+B_0+3\delta} \\ &= 1 - \frac{3(X_0+\delta)}{R_0+G_0+B_0+3\delta} = \frac{I_0-X_0}{I_{\text{new}}}. \end{aligned} \tag{8b}$$

Obviously, the saturation value changes when $I_{\text{new}} \neq I_0$. The difference between these two saturation values is

$$\begin{aligned} \Delta S = S' - S_0 &= \left(\frac{I_0-X_0}{I_{\text{new}}}\right) - \left(\frac{I_0-X_0}{I_0}\right) \\ &= -(I_0-X_0)\frac{\delta}{I_{\text{new}} \times I_0}. \end{aligned} \tag{9}$$

Since X_0 is the smallest value among R_0, G_0, and B_0, $I_0 - X_0$ in Eq. (9) must be positive. Hence, ΔS is negative if δ is positive and vice versa. Consequently, δ is crucial in the color distortion problem. Since I_{new} rarely equals I_0, δ is not generally equal to zero. At this point, the saturation value (S') of the fused image is different from the saturation value (S_0) of the resized original multispectral image. Therefore, the color distortion problem appears.

4. A new look at IHS-like image fusion

4.1. IHS image fusion

The IHS [1–3] is one of the widespread image fusion methods in the remote sensing community and has been employed as a standard procedure in many commercial packages. According to the fusion framework described in the previous section, we know that IHS is the intrinsic method in GIHS when I_{new} is replaced by the high-resolution Pan image. Following Eq. (5), a computationally efficient IHS method without the coordinate transformation can be given as

$$\begin{bmatrix} R_{\text{new}} \\ G_{\text{new}} \\ B_{\text{new}} \end{bmatrix} = \begin{bmatrix} 1 & -1/\sqrt{2} & 1/\sqrt{2} \\ 1 & -1/\sqrt{2} & -1/\sqrt{2} \\ 1 & \sqrt{2} & 0 \end{bmatrix} \begin{bmatrix} \text{Pan} \\ v1_0 \\ v2_0 \end{bmatrix} = \begin{bmatrix} R_0+\delta \\ G_0+\delta \\ B_0+\delta \end{bmatrix}, \tag{10}$$

where $\delta = \text{Pan} - I_0$.

Until now, most literatures recognized IHS as an order three method because it employs a 3×3 matrix as its transform kernel. A merit of the method proposed herein lies not only on its fast computing capability for fused images but also its ability to extend traditional three order transformations to arbitrary order. That is,

$$F_i = M_i + \beta, \tag{11}$$

where M_i denotes the resized hyperspectral or multispectral image of band i, $\beta = \text{Pan} - \kappa$, $\kappa = ((1/l)\sum_{i=1}^{l} M_i)$, and l represents the order or the number of bands.

Image fusion techniques with an arbitrary order are advantageous because they can easily handle higher order remote sensing images like hyperspectral or multispectral images with more than three bands.

4.2. Brovey transform

The BT is a simple image fusion method that preserves the relative spectral contributions of each pixel but replaces its overall brightness with the high-resolution panchromatic image. BT is defined as

$$\begin{bmatrix} R_{\text{new}} \\ G_{\text{new}} \\ B_{\text{new}} \end{bmatrix} = \gamma \cdot \begin{bmatrix} R_0 \\ G_0 \\ B_0 \end{bmatrix} = \frac{\text{Pan}}{I_0} \begin{bmatrix} R_0 \\ G_0 \\ B_0 \end{bmatrix}, \tag{12}$$

where $\gamma = \text{Pan}/I_0$. To evaluate the saturation effect of this transform, Eqs. (1) and (2) can be substituted into Eq. (12) to obtain an IHS-like form as follows:

$$\begin{bmatrix} R_{\text{new}} \\ G_{\text{new}} \\ B_{\text{new}} \end{bmatrix} = \gamma \cdot \begin{bmatrix} 1 & -1/\sqrt{2} & 1/\sqrt{2} \\ 1 & -1/\sqrt{2} & -1/\sqrt{2} \\ 1 & \sqrt{2} & 0 \end{bmatrix} \begin{bmatrix} I_0 \\ v1_0 \\ v2_0 \end{bmatrix} = \begin{bmatrix} 1 & -1/\sqrt{2} & 1/\sqrt{2} \\ 1 & -1/\sqrt{2} & -1/\sqrt{2} \\ 1 & \sqrt{2} & 0 \end{bmatrix} \begin{bmatrix} \text{Pan} \\ \gamma \cdot v1_0 \\ \gamma \cdot v2_0 \end{bmatrix}. \quad (13)$$

Eq. (13) demonstrates that although the hue for the fused image using BT is unchanged. However, the saturation value is changed from S_0 to

$$S'' = \gamma \cdot \sqrt{v1_0^2 + v2_0^2} = \gamma \cdot S_0. \quad (14)$$

In summary, both the IHS and BT are linear image fusion method. They keep the same spatial resolution as the Pan image but distort the spectral (color) characteristics. When I_0 is replaced by Pan, the saturation relationship among IHS, BT and GIHS can be given by

$$S_0 = \gamma \cdot S' \quad \text{for the IHS and GIHS method} \quad (15)$$

and

$$S'' = \gamma^2 \cdot S' \quad \text{for Brovey transform and GIHS method.} \quad (16)$$

Consequently, the color distortion problem is the worst resulted by the BT and slightly better by the IHS method.

4.3. Principal components analysis

The PCA technique [2–4], also known as the Karhunen–Loeve transform, is a decorrelation scheme used for various mapping and information extraction in remote sensing image data. It is possible to derive an orthogonal color coordinate system for PCA which is given below:

$$\begin{bmatrix} \text{PC1} \\ \text{PC2} \\ \text{PC3} \end{bmatrix} = \begin{bmatrix} \phi_{11} & \phi_{12} & \phi_{13} \\ \phi_{21} & \phi_{22} & \phi_{23} \\ \phi_{31} & \phi_{32} & \phi_{33} \end{bmatrix} \begin{bmatrix} R_0 \\ G_0 \\ B_0 \end{bmatrix} \quad (17a)$$

$$H = \tan^{-1}\left(\frac{\text{PC3}}{\text{PC2}}\right) \quad \text{and} \quad S = \sqrt{\text{PC2}^2 + \text{PC3}^2}. \quad (17b)$$

The hue and saturation defined here are different to the IHS system in Eq. (2). The transformation matrix $\boldsymbol{\Phi}$ composed of term ϕ_{ij}, consists of the eigenvectors of the covariance matrix of the RGB vectors. Let $\boldsymbol{R}$ represents the covariance matrix with general terms r_{ij}, then the transformation matrix satisfies the relationship

$$\boldsymbol{\Phi R \Phi}^{\text{T}} = \boldsymbol{\Lambda}, \quad (18)$$

where $\boldsymbol{\Lambda} = \text{diag}(\Lambda_1, \Lambda_2, \Lambda_3)$ are eigenvalues corresponding to $\boldsymbol{\Phi}$ with a descend order.

The procedure to merge the RGB and the Pan image using the PCA method is similar to that of the IHS method. That is, the first component (PC1) of the PCA space is replaced by the Pan image and retransformed back into the original RGB space:

$$\begin{bmatrix} R_{\text{new}} \\ G_{\text{new}} \\ B_{\text{new}} \end{bmatrix} = \begin{bmatrix} \phi_{11} & \phi_{21} & \phi_{31} \\ \phi_{12} & \phi_{22} & \phi_{32} \\ \phi_{13} & \phi_{23} & \phi_{33} \end{bmatrix} \begin{bmatrix} \text{Pan} \\ \text{PC2} \\ \text{PC3} \end{bmatrix}. \quad (19)$$

Since PCA depends on the second-order statistics of the data, to evaluate the color effect of the PCA fusion with IHS and BT methods becomes a difficult task. Furthermore, it is hard to describe the transformation characteristics by using the eigenvectors in $\boldsymbol{\Phi}$. Herein we use a well-known data independent transform, pseudo KL transform (PKLT) [17] to illustrate PCA fusion. The PKLT is represented by

$$\begin{bmatrix} \text{PPC1} \\ \text{PPC2} \\ \text{PPC3} \end{bmatrix} = \begin{bmatrix} 1/3 & 1/3 & 1/3 \\ 1/2 & 0 & -1/2 \\ -1/4 & 1/2 & -1/4 \end{bmatrix} \begin{bmatrix} R \\ G \\ B \end{bmatrix}. \quad (20)$$

In a similar manner, the PKLT image fusion can be constructed by replacing the first component (PPC1) by Pan. That is,

$$\begin{bmatrix} R_{\text{new}} \\ G_{\text{new}} \\ B_{\text{new}} \end{bmatrix} = \begin{bmatrix} 1 & 1 & -2/3 \\ 1 & 0 & 4/3 \\ 1 & -1 & -2/3 \end{bmatrix} \begin{bmatrix} \text{Pan} \\ \text{PPC2} \\ \text{PPC3} \end{bmatrix} = \begin{bmatrix} \text{Pan} \\ \text{Pan} \\ \text{Pan} \end{bmatrix} + \begin{bmatrix} 1 & -2/3 \\ 0 & 4/3 \\ -1 & -2/3 \end{bmatrix} \begin{bmatrix} \text{PPC2} \\ \text{PPC3} \end{bmatrix} = \begin{bmatrix} R_0 + \delta' \\ G_0 + \delta' \\ B_0 + \delta' \end{bmatrix}, \quad (21)$$

where $\delta' = \text{Pan} - \text{PPC1}$.

In most cases, the eigenvector structures of a real multispectral image are similar to that of the transform kernel in Eq. (20), i.e., they have the same zero-crossing numbers. Ideally, Eq. (19) can be approximated to the following form:

$$\begin{bmatrix} R_{\text{new}} \\ G_{\text{new}} \\ B_{\text{new}} \end{bmatrix} = \begin{bmatrix} \phi_{11} & \phi_{21} & \phi_{31} \\ \phi_{12} & \phi_{22} & \phi_{32} \\ \phi_{13} & \phi_{23} & \phi_{33} \end{bmatrix} \begin{bmatrix} \text{Pan} \\ \text{PC2} \\ \text{PC3} \end{bmatrix} = \begin{bmatrix} \text{Pan}' \\ \text{Pan}' \\ \text{Pan}' \end{bmatrix} + \begin{bmatrix} \phi_{21} & \phi_{31} \\ \phi_{22} & \phi_{32} \\ \phi_{23} & \phi_{33} \end{bmatrix} \begin{bmatrix} \text{PC2} \\ \text{PC3} \end{bmatrix} \cong \begin{bmatrix} \text{Pan} \\ \text{Pan} \\ \text{Pan} \end{bmatrix} + \begin{bmatrix} \phi_{21} & \phi_{31} \\ \phi_{22} & \phi_{32} \\ \phi_{23} & \phi_{33} \end{bmatrix} \begin{bmatrix} \text{PC2} \\ \text{PC3} \end{bmatrix} \approx \begin{bmatrix} R_0 + \delta'' \\ G_0 + \delta'' \\ B_0 + \delta'' \end{bmatrix}, \quad (22)$$

where $\delta'' \approx \text{Pan} - \text{PC1}$. However, $\text{Pan}' = \text{Pan}$ only when the first eigenvector $[\phi_{11}\ \phi_{12}\ \phi_{13}]$ equals to $[1/3\ 1/3\ 1/3]$.

By observing Eqs. (21) and (22), it can be noted that both methods kept the similar spatial resolution, but with different saturation distortion. According to Eq. (21), the first component (PPC1) in PKLT is just equal

to the intensity component I_0 in IHS. That is, the effect of saturation resulted in PKLT and IHS is the same. To compare the color distortion in PKLT and PCA fusion, we can directly compare the values of δ' and δ''. Due to the fact that PPC1 represents the mean image of the low-resolution color image while PC1 stands for the largest variance image. Intuitively, δ'' is smaller than δ' since PC1 achieves more spatial details than PPC1. In other words, PC1 has similar correlation with the Pan image. This argument agrees with Chavez's experiments [2]. Hence, PCA fusion distorts the spectral characteristics least because the saturation shift ΔS in PCA is the smallest among these three methods.

4.4. Wavelet image fusion

As a powerful analytical tool, wavelet-based methods have been recently developed for signal and image processing. More recently, wavelets have started playing a role in image fusion. The original principle of the wavelet image fusion is to get the best resolution without altering the spectral contents of the image. More clearly, this principle is based on multiresolution analysis provided by the wavelet transforms [18]. Typical wavelets for image fusion are usually dyadic in image space, hence the image size is often limited to a power of 2. To resolve this restriction, Jorge et al. [7–11] proposed an "à trous" algorithm with $\mathbf{B}_3$ cubic spline function and two to three level decomposition for the image fusion.

An "à trous"-based, wavelet image fusion can be accomplished by two different approaches, i.e., substitution and additive approaches. Wavelet substitution method (WS) [7,10,11] substitutes the details of multispectral images by those of the panchromatic image, and then combines them with the residual multispectral images. That is,

$$\begin{bmatrix} R_{\text{new}} \\ G_{\text{new}} \\ B_{\text{new}} \end{bmatrix} = \begin{bmatrix} R_{\text{r}} \\ G_{\text{r}} \\ B_{\text{r}} \end{bmatrix} + \begin{bmatrix} \sum_{k=1}^{n} W_{\text{P}k} \\ \sum_{k=1}^{n} W_{\text{P}k} \\ \sum_{k=1}^{n} W_{\text{P}k} \end{bmatrix} = \begin{bmatrix} R_{\text{r}} \\ G_{\text{r}} \\ B_{\text{r}} \end{bmatrix} + \begin{bmatrix} \delta_{\text{P}} \\ \delta_{\text{P}} \\ \delta_{\text{P}} \end{bmatrix} \tag{23a}$$

which satisfies

$$\text{Pan} = \sum_{k=1}^{n} W_{\text{P}k} + \text{Pan}_{\text{r}} = \delta_{\text{P}} + \text{Pan}_{\text{r}} \tag{23b}$$

and

$$\begin{bmatrix} R_0 \\ G_0 \\ B_0 \end{bmatrix} = \begin{bmatrix} R_{\text{r}} \\ G_{\text{r}} \\ B_{\text{r}} \end{bmatrix} + \begin{bmatrix} \sum_{k=1}^{n} W_{\text{R}k} \\ \sum_{k=1}^{n} W_{\text{G}k} \\ \sum_{k=1}^{n} W_{\text{B}k} \end{bmatrix} = \begin{bmatrix} R_{\text{r}} \\ G_{\text{r}} \\ B_{\text{r}} \end{bmatrix} + \begin{bmatrix} \delta_{\text{R}} \\ \delta_{\text{G}} \\ \delta_{\text{B}} \end{bmatrix}, \tag{23c}$$

where $\delta_{\text{P}} = \sum_{k=1}^{n} W_{\text{P}k} = \text{Pan} - \text{Pan}_{\text{r}}$ denotes the multiresolution wavelet plane, and Pan_{r} is the smooth version of Pan. In fact, δ_{P} can be regarded as the spatial details of the Pan image. δ_{R}, δ_{G} and δ_{B} are the successive level details of the R_0, G_0, and B_0 images, respectively. R_{r}, G_{r} and B_{r} are the residual multispectral images.

In the Wavelet additive (WA) method [7,10–12], the successive level details of panchromatic image are directly added to the multispectral image as follows. This is relatively an easy method.

$$\begin{bmatrix} R_{\text{new}} \\ G_{\text{new}} \\ B_{\text{new}} \end{bmatrix} = \begin{bmatrix} R_0 \\ G_0 \\ B_0 \end{bmatrix} + \begin{bmatrix} \delta_{\text{P}} \\ \delta_{\text{P}} \\ \delta_{\text{P}} \end{bmatrix}. \tag{24}$$

To evaluate the effect of saturation in the WA image fusion, Eqs. (1) and (2) can be substituted into Eq. (24) to obtain an IHS-like form which is given below:

$$\begin{aligned} \begin{bmatrix} R_{\text{new}} \\ G_{\text{new}} \\ B_{\text{new}} \end{bmatrix} &= \begin{bmatrix} R_0 \\ G_0 \\ B_0 \end{bmatrix} + \begin{bmatrix} \delta_{\text{P}} \\ \delta_{\text{P}} \\ \delta_{\text{P}} \end{bmatrix} \\ &= \begin{bmatrix} 1 & -1/\sqrt{2} & 1/\sqrt{2} \\ 1 & -1/\sqrt{2} & -1/\sqrt{2} \\ 1 & \sqrt{2} & 0 \end{bmatrix} \begin{bmatrix} I_0 + \delta_{\text{P}} \\ v1_0 \\ v2_0 \end{bmatrix} \\ &= \begin{bmatrix} I_{\text{new}} \\ I_{\text{new}} \\ I_{\text{new}} \end{bmatrix} + \begin{bmatrix} -1/\sqrt{2} & 1/\sqrt{2} \\ -1/\sqrt{2} & -1/\sqrt{2} \\ \sqrt{2} & \sqrt{0} \end{bmatrix} \begin{bmatrix} v1_0 \\ v2_0 \end{bmatrix}, \end{aligned} \tag{25}$$

where $I_{\text{new}} = I_0 + \delta_{\text{P}}$.

Characteristically, Eq. (25) indicates that the WA method does not use the Pan image but I_{new} to replace I_0. This equation suggests that the spatial quality of the merged image by the WA method is obviously less than those by traditional methods, since the spatial details extracted by I_{new} are always less than those in the Pan

Fig. 1. The panchromatic SPOT image.

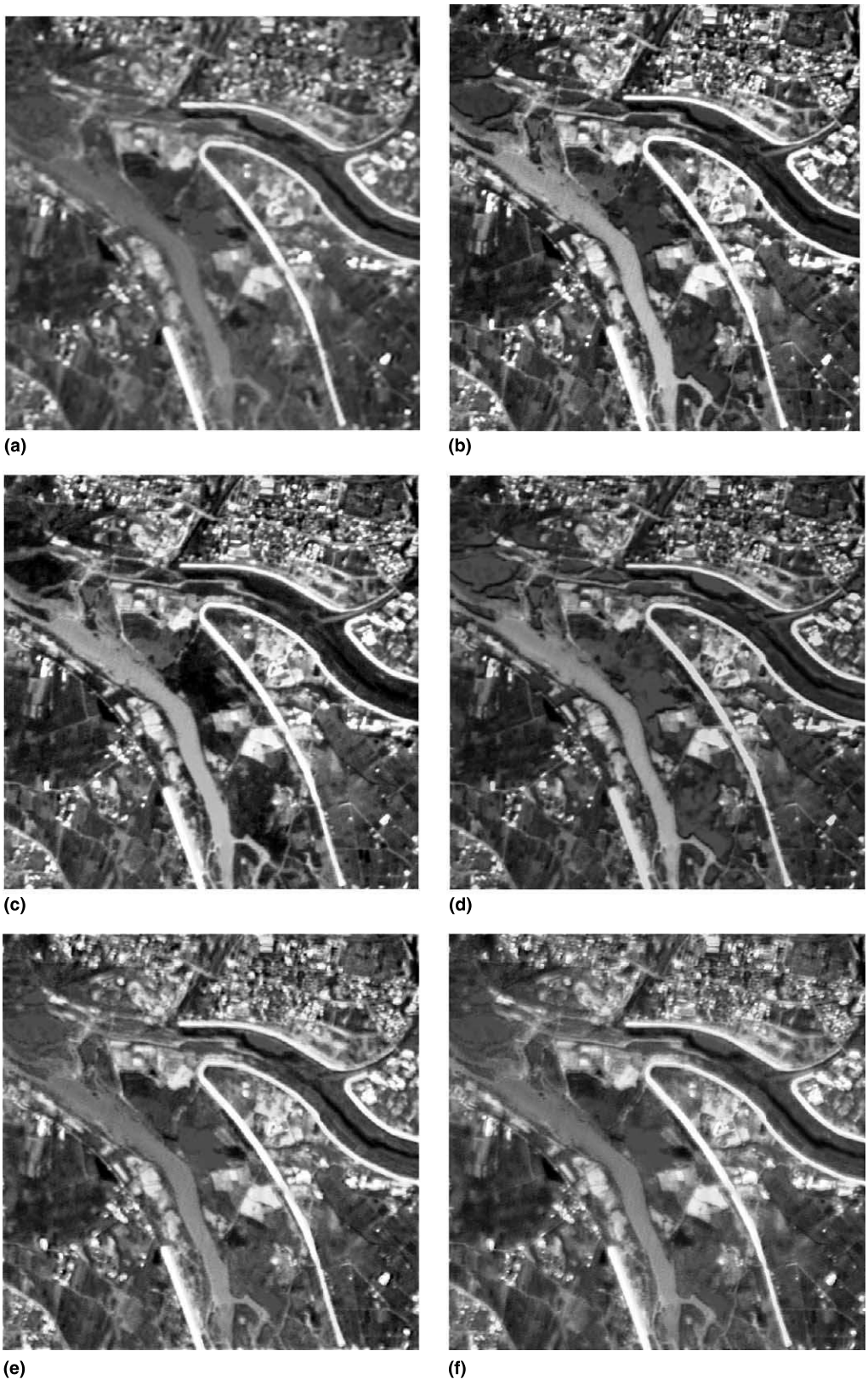

Fig. 2. (a) Color composite of the resized SPOT XS image. Color composite of the fused image using (b) IHS, (c) BT, (d) PCA, (e) WA, (f) WS.

Table 1
The correlation coefficients between three-color (R, G, and B) resized SPOT images and images fused by distinct methods and their average values

	R	G	B	Average
IHS	0.7692	0.8824	0.8657	0.8391
BT	0.5095	0.8751	0.8781	0.7542
PCA	0.8315	0.8836	0.9039	0.8730
WA	0.9704	0.9759	0.9719	0.9727
WS	0.9589	0.9651	0.9559	0.9599

Table 2
The correlation coefficients between the panchromatic image and the intensity image of the merged image

IHS	BT	PCA	WA	WS
0.9848	0.9955	0.9572	0.8553	0.8810

image. In contrast to the other IHS-like methods, the value of δ_P in WA is adjustable rather than a fixed value. The larger the value of δ_P, the more spatial content of the high-resolution panchromatic image is embedded into the merged image and produces more distorted saturation, and vice versa.

On the other hand, the WS method substitutes the details of color image by those of panchromatic image. However, the extra decomposition in the color image can not certify a higher fusion quality. To verify this fact, another color shift, $\delta_{R,G,B}$ in Eq. (23c) is substituted into Eq. (8b) and the result is given below:

Fig. 3. The panchromatic IKONOS image.

$$
\begin{aligned}
S'_{WS} &= 1 - \frac{3\min(R_r + \delta_P, G_r + \delta_P, B_r + \delta_P)}{R_r + G_r + B_r + 3\delta_P} \\
&= 1 - \frac{3(X'_0 + \delta_P)}{R_0 + G_0 + B_0 + 3\delta_P - (\delta_R + \delta_G + \delta_B)} \\
&= \frac{I - X'_0 - \Delta X}{I_{new} - \Delta X} \approx \frac{I - X'_0}{I_{new}} \\
&= 1 - \frac{3\min(R_0 + \delta_P, G_0 + \delta_P, B_0 + \delta_P)}{R_0 + G_0 + B_0 + 3\delta_P} \\
&= S'_{WA}, \qquad (26)
\end{aligned}
$$

where $\Delta X = (\delta_R + \delta_G + \delta_B)/3$, X'_0 is the smallest value among R_r, G_r, and B_r.

Consequently, the wavelet methods reveal that the "additive" method gives a simple, fast, and efficient fusion process than the "substitution" one, since the "additive" wavelet method for image fusion does not decompose the multispectral image but just add the details of panchromatic image into the multispectral image.

5. Experimental results

The most widely applied fusion procedure is the merging of panchromatic SPOT image with three-color SPOT imagery or multispectral LANDSAT TM imagery. The first experiment presents an example of a fused SPOT image to highlight the color distortion problem. The test images used herein includes a 10-m resolution panchromatic image and three 20-m color images of a rural area in Taichung, Taiwan collected on March 4, 1994 by the SPOT satellite. The size of the test image is 512×512 pixels for the panchromatic image as displayed in Fig. 1. Fig. 2(a) presents the resized three-color imagery. Figs. 2(b)–(f) illustrate the fusion results by IHS, BT, PCA, WA, and WS, respectively. By considering spatial effect it reveals that the results of the three former methods (IHS, BT and PCA) share the similar details. River, houses, streets and so on are evident in the fused images when using all these three methods. However, some of the spatial details extracted by the wavelet-based methods are lost. Compared to the original color image, Fig. 2(b), the color of the fused images obtained by IHS and BT is obviously distorted (with red darkening). Distortion of the spectral characteristics resulted by the BT method is the most. On the other hand, the PCA, WA and WS methods provide good color effect. The red areas in these three images have almost the same color and brightness as those in the original three-color SPOT imagery. Meanwhile, the color of the residential areas is almost identical.

At present, no quantitative methods have been found in current literature to evaluate the performance of various image fusion techniques. Most of the evaluation

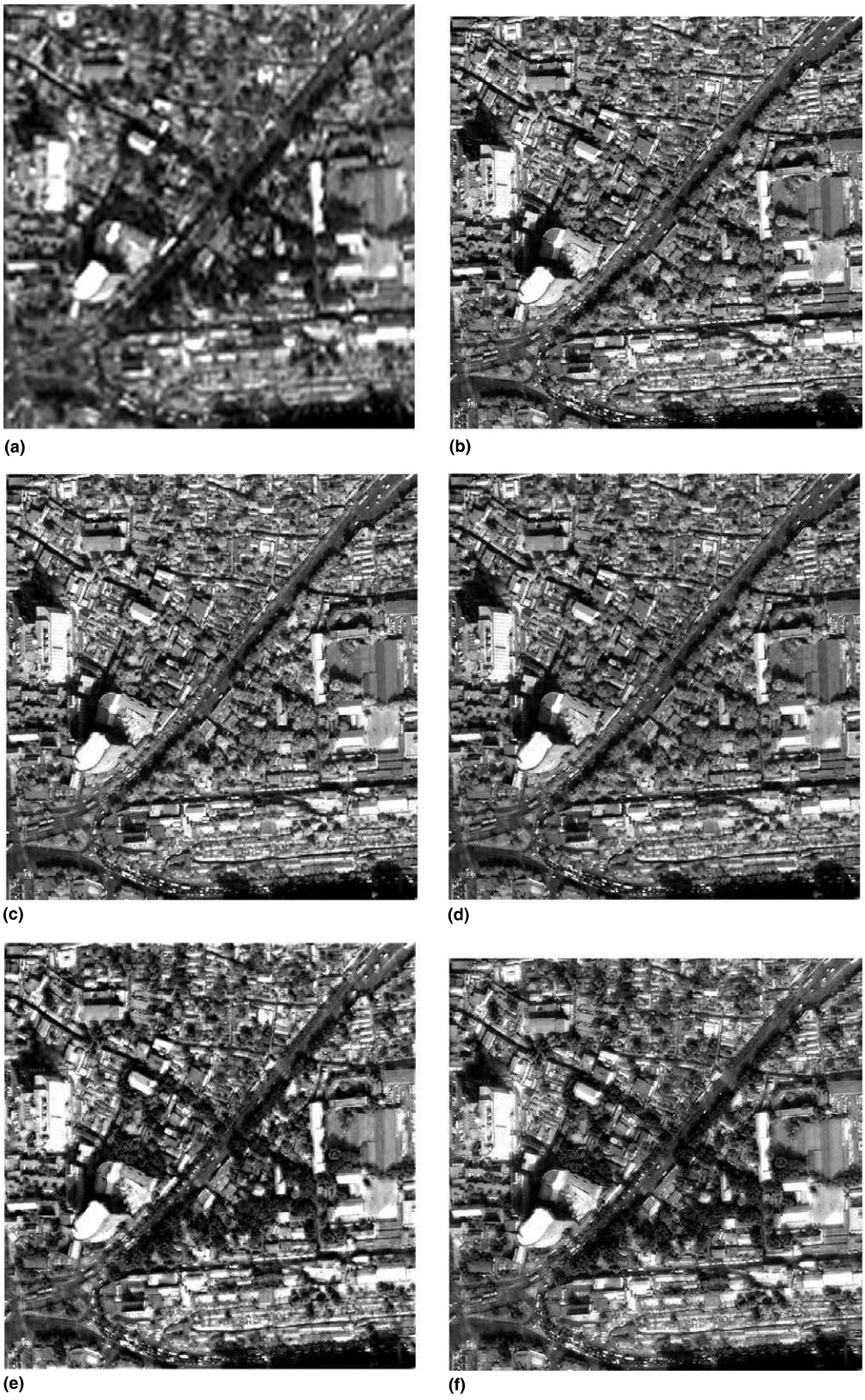

Fig. 4. (a) Color composite of the resized multispectral IKONOS image. Color composite of the fused image using (b) IHS, (c) BT, (d) PCA, (e) WA, (f) WS.

Table 3
The correlation coefficients between three-color (R, G, and B) resized IKONOS images and images fused by distinct methods and their average values

	R	G	B	Average
IHS	0.7374	0.7222	0.6916	0.7171
BT	0.7033	0.6982	0.7399	0.7138
PCA	0.7162	0.7206	0.7509	0.7292
WA	0.9037	0.8978	0.8889	0.8968
WS	0.8907	0.8842	0.8722	0.8824

Table 4
The correlation coefficients between the panchromatic image and the intensity image of the merged image

IHS	BT	PCA	WA	WS
0.9997	0.9992	0.9971	0.8870	0.8980

is based on visual examination. In this work we use the correlation coefficients between the original resized three-color imagery and the merged three-color image as an index for the correctness of spectral quality. For spatial quality evaluation, we have calculated the correlation coefficients between the panchromatic image and the intensity image of the merged image as another index. Correlation coefficients for all these five image fusion methods are depicted in Tables 1 and 2.

Table 1 demonstrates the correlation coefficients between three-color (R, G, and B) resized SPOT images and images fused by distinct methods and their average values. Although most of these values do not have much difference, they can be separated into two distinct groups. The first group includes three methods, i.e. IHS, BT, and PCA. Apart from the worst case, most values are around 0.7–0.9. The second group consists of two wavelet image fusion methods with their values all greater than 0.95. These metrics verify our previous discussion that the image fusion by IHS, BT, and PCA have color distortion problem to some degree but wavelet methods can preserve the spectral characteristics better. Table 2 indicates the spatial correlation coefficients for these five image fusion methods. Interestingly, groups in these two tables are consistent but their properties are quite different (in opposite manner). All correlation coefficients of the group of IHS, BT, and PCA are greater than 0.95 while those of WA and WS are around 0.8–0.9. In summary, these two groups represent two distinct approaches with different strength and drawbacks. The IHS, BT, and PCA can preserve almost all of spatial information that Pan has in the fused image but must face color distortion problem, which is the worst resulted by BT. Alternatively, WA and WS can preserve the spectral information that multispectral images have but produce blurred fused images. Similar results were obtained in the following experiment.

The second experiment conducted in this section is based on the new CARTERRA image. The test images, a 1 m resolution panchromatic and three 4 m color images of Beijing, China were collected on October 22, 1999 by Space Imaging's IKONOS satellite. Fig. 3 displays the test panchromatic image while Fig. 4(a) presents its resized multispectral image (using R, G and B bands only). Meanwhile, Figs. 4(b)–(f) illustrate the fusion results by these five techniques. The corresponding correlation coefficients are tabulated in Tables 3 and 4. Comparing these two experiments, it can be noted that the visual and quantitative results from the CARTERRA image are similar to SPOT image. Although ranges of correlation coefficients shown in Tables 1 and 2 with respect to Tables 3 and 4 are different, the group members and their properties in these four tables are identical.

A more detailed inspection reveals that although the spatial quality of the IHS, BT and PCA are almost identical, a subtle distinction still exists as the spatial details of the Pan′ image in PCA are less than the spatial details of the Pan image in IHS and BT. Therefore, the spatial quality of the merged image by PCA is slightly worse than that by IHS and BT. Meanwhile, the distortion of the spectral characteristics by BT method is the highest and the least by PCA method among these traditional methods. Further experiments using the SPOT and CARTERRA image also reach similar conclusions. The optimal level decomposition for the WT-based image fusion to get the best resolution without altering the spectral contents of the image is three to four. More or less levels in decomposition lead to a degeneration of either spatial quantity or spectral characteristics.

6. Conclusions

Various image fusion techniques have been conducted to merge different sensor data. With the development of new imaging sensors, however, image fusion becomes an important technique, which is capable of quickly merging the massive volume of data while simultaneously preserving most information. Until now, these contemporary methods have only been independently evaluated by some statistical metrics, and have seldom been compared quantitatively with each other, in both spectral and spatial features. To evaluate these methods, this work starts from modeling the color space of image, and presents a relatively detailed study indicating that all of the IHS, BT, PCA, and wavelet-based methods can be regarded as an IHS-like method. We also indicate that they have color distortion problem arising from the change of the saturation during the fusion process. Experiments with several SPOT and CARTERRA data sets confirmed that the proposed

viewpoints are highly reliable and also serve as a reference to design new algorithms for image fusion.

Acknowledgements

The authors would like to thank Space Imaging company for providing the IKONOS data. We also thank the National Science Council of the Republic of China for financial support under Contract No. NSC 89-2213-E-014-013. Finally, the authors would like to thank the anonymous reviewers for their comments which helped to improve the paper quality and presentation.

References

[1] W.J. Carper, T.M. Lillesand, R.W. Kiefer, The use of intensity-hue-saturation transformations for merging SPOT panchromatic and multispectral image data, Photogramm. Eng. Remote Sensing 56 (1990) 459–467.
[2] P.S. Chavez Jr., S.C. Sides, J.A. Anderson, Comparison of three difference methods to merge multiresolution and multispectral data: Landsat TM and SPOT panchromatic, Photogramm. Eng. Remote Sensing 57 (1991) 295–303.
[3] E. Kathleen, A.D. Philip, The use of intensity-hue-saturation transformation for producing color shaded relief images, Photogramm. Eng. Remote Sensing 60 (1994) 1369–1374.
[4] P.S. Chavez, A.Y. Kwarteng, Extracting spectral contrast in Landsat thematic mapper image data using selective principal component analysis, Photogramm. Eng. Remote Sensing 55 (1989) 339–348.
[5] P. Blanc, T. Blus, T. Ranchin, L. Wald, R. Aloisi, Using iterated rational filter banks within the ARSIS concepts for producing 10 m Landsat multispectral images, Int. J. Remote Sensing 19 (1998) 2331–2343.
[6] T. Ranchin, L. Wald, Fusion of high spatial and spectral resolution images: the ARSIS concept and its implementation, Photogramm. Eng. Remote Sensing 66 (2000) 49–61.
[7] N. Jorge, O. Xavier, F. Octavi, P. Albert, P. Vicenc, A. Roman, Multiresolution-based imaged imaged fusion with additive wavelet decomposition, IEEE Trans. Geosci. Remote sensing 37 (1999) 1204–1211.
[8] C. Pohl, J.L. Van Genderen, Multisensor image fusion in remote sensing: concepts, methods and applications, Int. J. Remote Sensing 19 (1998) 823–854.
[9] ER Mapper 5.0 Reference, Earth Resource Mapping Pty Ltd, 1995.
[10] D.A. Yocky, Multiresolution wavelet decomposition image merge of Landsat Thematic Mapper and SPOT panchromatic data, Photogramm. Eng. Remote Sensing 62 (1996) 1067–1074.
[11] N. Jorge, O. Xavier, F. Octavi, P. Albert, Simultaneous image fusion and reconstruction using wavelets application to SPOT + LANDSAT images, Vistas Astron. 41 (1997) 351–357.
[12] B.G. Duport, J. Girel, J.M. Chassery, G. Pautou, The use of multiresolution analysis and wavelets transform for merging SPOT panchromatic and multispectral image data, Photogramm. Eng. Remote Sensing 62 (1996) 1057–1066.
[13] T. Ranchin, L. Wald, The wavelet transform for analysis of remotely sensed images, Int. J. Remote Sensing 14 (1993) 615–619.
[14] R.C. Gonzalez, R.E. Woods, Digital Image Processing, Addison-Wesley, Reading, MA, 1992.
[15] W.K. Pratt, Digital Image Processing, second ed., Wiley, New York, 1991.
[16] R.S. Ledley, M. Buas, T.J. Golab, Fundamentals of true-color image processing, Proc. Int. Conf. Pattern Recognition 1 (1990) 791–795.
[17] R.M. Haralick, L.G. Shapiro, Computer and Robot Vision, Addison-Wesley, Reading, MA, 1992.
[18] S. Mallat, A Wavelet Tour of Signal Processing, Academic Press, New York, 1998.